Contents lists available at ScienceDirect

# **Electric Power Systems Research**

journal homepage: www.elsevier.com/locate/epsr



# Check for updates

# Quantum microgrid state estimation<sup>∞</sup>

Fei Feng, Peng Zhang\*, Yifan Zhou, Zefan Tang

Electrical and Computer Engineering, Stony Brook University, Stony Brook, NY, USA

#### ARTICLE INFO

Keywords: Quantum computing State estimation Hierarchical control Microgrid

#### ABSTRACT

This paper investigates the feasibility and efficiency of quantum-circuit-based algorithms for microgrid state estimation. Our new contributions include: (1) a general quantum state estimation (GQSE) formulation is devised for swing-bus-contained microgrids through the quantized Gaussian–Newton iteration, (2) a preconditioned quantum linear solver (PQLS) is developed for tackling the ill-conditioned GQSE with limited quantum resources, and (3) an enhanced quantum state estimation (EQSE) algorithm is further established for hierarchical-control-based microgrids with exogenous disturbances. Extensive case studies demonstrate the correctness of GQSE, PQLS and EQSE in two typical microgrids. The robustness and convergence performance of EQSE are also verified.

## 1. Introduction

Microgrid is a proven paradigm that can flexibly manage distributed energy resources (DERs) and ensure the electricity resiliency against outages [1,2]. Among many microgrid functions, state estimation is of fundamental importance as it enables online monitoring and control of microgrids based on a limited number of sensors such as microPMUs (micro-phasor measurement units). The basic requirements for microgrid state estimation mainly include accuracy, efficiency, and resiliency against noises [3]. For modern microgrids, an increasingly urgent and important demand is the need of high-frequency state estimation due to the community expansion, a high penetration of uncertain renewables, and volatile operational conditions [4]. However, the complexities of almost all the classical state estimation methods scale polynomially with the problem size, which makes those methods no longer suitable for a future grid with formidable real-time operation needs.

To overcome the complexity issue, quantum computing provides a promising solution. Unlike classical computing, quantum computing requires fewer bits (i.e., qubits) to handle a complicated problem. For microgrid state estimation, a main bottleneck is to establish an efficient solver for a sparse linear system of equations. Currently, there are mainly two types of quantum linear system algorithms: hybrid quantum/classical algorithms and quantum-circuit-based algorithms [5,6]. Hybrid algorithms are developed for the noisy intermediate-scale quantum (NISQ) era. Examples include the Variational Quantum Linear

Solver and quantum random walk algorithms [7,8]. Specifically, a hybrid algorithm utilizes the interaction between quantum and classical computers such that the quantum circuit depth is effectively reduced to accommodate the high noise level and short coherence time on NISQ devices. However, the inevitable computation and optimization processes on classical computers have made most hybrid algorithms heuristic. As a consequence, the convergence and efficiency of hybrid algorithms cannot be strictly guaranteed.

Quantum-circuit-based algorithms enable exponential speedups over traditional methods on noise-free quantum computers [5,9]. An important milestone in recent years has been the development of the Harrow–Hassidim–Lloyd (HHL) algorithm, a pure quantum method for solving linear equations. Specifically, the HHL algorithm utilizes a unitary transformation to prepare a quantum superposition for a linear system solution [10]. Several HHL variants have also been studied for enhanced convergence precision [11] and enhanced robustness under different conditions [12,13]. A salient feature of HHL (or any of its variants) is that it effectively accelerates the analysis of a sparse system, which exactly matches the characteristics of power systems. In our prior work [14,15], we have used HHL to devise dynamic/static-state-related quantum algorithms for power flow and electromagnetic transients analyses.

In addition to the complexity issue, high-volume state measurement and information exchange also make microgrids vulnerable to

E-mail addresses: fei.feng@stonybrook.edu (F. Feng), p.zhang@stonybrook.edu (P. Zhang), yifan.zhou.1@stonybrook.edu (Y. Zhou), zefan.tang@stonybrook.edu (Z. Tang).

This work was supported in part by the Advanced Grid Modeling Program under the US Department of Energy's Office of Electricity, in part by the US National Science Foundation under Grant No. OIA-2040599, and in part by Stony Brook University's Office of the Vice President for Research through a Quantum Information Science and Technology Seed Grant.

<sup>\*</sup> Corresponding author.

exogenous disturbances [16]. The existing microgrid state estimation methods typically follow classical power flow formulations, which however have ignored the features of droop-based microgrids where multiple DERs, instead of a swing bus, support the entire system [17]. For instance, [18] presents a distributed state estimation approach for microgrids connected with distribution systems. For hybrid AC/DC microgrids, the state estimation problem is solved by decomposing the system into subsystems [19]. In those existing methods, microgrids are modeled in the same way with the traditional distribution feeders where a main grid or an infinite source is used to support the downstream system. Failure to represent the droop/secondary regulation may provide erroneous results when a microgrid is subject to unforeseeable disturbances.

In this paper, we investigate the feasibility and efficiency of quantum-circuit-based algorithms for microgrid state estimation. Specifically, we first devise a general quantum state estimation (GQSE) formulation for swing-bus-constrained microgrids through the quantized Gaussian–Newton iteration. To resolve the ill-conditioned matrix issue in GQSE, a preconditioned quantum linear solver (PQLS) is developed with limited quantum resources. Further, we establish an enhanced quantum state estimation (EQSE) algorithm for hierarchical-control-based microgrids with exogenous disturbances. These quantum algorithms are conducted through IBM's Qiskit, Terra, and the IBMQ provider. A traditional state estimation method is implemented in MAT-LAB for comparison. Extensive case studies demonstrate the correctness of GQSE, PQLS and EQSE in two typical microgrids, and the robustness and convergence performance of EQSE are also verified.

The rest of this paper is organized as follows: Section 2 and III describe the GQSE formulation and PQLS, respectively. The EQSE algorithm is presented in Section 4. Section 5 provides our test results. Section 6 concludes the paper.

## 2. GQSE for microgrids

This section presents the GQSE formulation. Without loss of generality, a DC microgrid is studied in this paper, yet the formulation can be readily extended to AC microgrids.

## 2.1. GQSE formulation

State estimation is an indispensable functionality in modern energy management systems for determining power system states with raw measurement data containing heterogeneous noises [20]. The weighted least square is a widely used method for state estimation. It minimizes the sum of weighted squared errors between measurements and estimated system states. The following equation gives the cost function of state estimation for a DC microgrid:

$$J(V) = \left[z - h(V)\right]^{T} R^{-1} \left[z - h(V)\right], \tag{1}$$

where V denotes a vector of per-unit unknown bus voltages (to be determined, and the initialized V is a vector where each element is one). h(V) is a vector containing the system states to be estimated. In this study, the estimated system states consist of three types of states, namely, power injections at unknown-voltage buses, branch powers at unknown-voltage buses, and unknown voltages. Mathematically, it can be expressed as follows:

$$h(V) = \begin{bmatrix} P(V) \\ P_{(g,l)}(V) \\ V \end{bmatrix} = \begin{bmatrix} GV \circ V \\ V_{(g)} \circ g_{(g,l)} \circ (V_{(g)} - V_{(l)}) \\ V \end{bmatrix}, \tag{2}$$

where P(V) is a vector of power injections at unknown-voltage buses.  $P_{(g,l)}(V)$  denotes the branch-power vector.  $V_g$  and  $V_l$  are from-bus-voltage and to-bus-voltage vectors, respectively. G and  $g_{(g,l)}$  are the nodal conductance matrix and branch conductance vector of the DC microgrid, respectively.  $\circ$  indicates the Hadamard product.

In (1), z is a vector containing the measured results of variables in h(V). R is the weight matrix (each element in R represents the coefficient for the corresponding element in [z - h(V)]).

The Gauss–Newton algorithm can be applied to solving the non-linear least square problem in (1). It performs following iterations to obtain the minimal cost function:

$$H^{T}R^{-1}(z - h(V_{k-1})) = (H^{T}R^{-1}H)\Delta V_{k},$$
(3)

where  $\boldsymbol{V}_{k-1}$  denotes the bus-voltage vector at the (k-1)th iteration,  $\Delta \boldsymbol{V}_k$  is a vector at the kth iteration containing the difference between  $\boldsymbol{V}_k$  and  $\boldsymbol{V}_{k-1}$ , and  $\boldsymbol{H}$  is the Jacobian matrix of  $\boldsymbol{h}(\boldsymbol{V}_{k-1})$ . Then, the bus-voltage vector  $\boldsymbol{V}_k$  can be updated as  $\boldsymbol{V}_k = \boldsymbol{V}_{k-1} + \Delta \boldsymbol{V}_k$ .

The major computation burden of the Gauss–Newton algorithm lies in (3), which involves the calculation of the gain matrix inverse, i.e.,  $(\boldsymbol{H}^T \boldsymbol{R}^{-1} \boldsymbol{H})^{-1}$ . Meanwhile, the gain matrix  $\boldsymbol{H}^T \boldsymbol{R}^{-1} \boldsymbol{H}$  inherits the sparsity feature from the Jacobian matrix  $\boldsymbol{H}$  and is strictly Hermitian. This allows the classical state estimation to be converted to a quantum formulation.

In the GQSE formulation, the HHL algorithm is utilized to tackle (3) to reduce the computational complexity of the entire state estimation. For concision, the following derivations omit the subscript k. The classical formulation (3) can be converted to a quantum computing model as follows:

$$|\mathbf{H}^T \mathbf{R}^{-1} (\mathbf{z} - \mathbf{h}(\mathbf{V}))\rangle = (\mathbf{H}^T \mathbf{R}^{-1} \mathbf{H}) |\Delta \mathbf{V}\rangle, \tag{4}$$

where  $|\Delta V\rangle$  is a normalized quantum state of  $\Delta V$ . To be specific, the *i*th component of  $\Delta V$  corresponds to the amplitude of the *i*th basis state of the quantum state  $|\Delta V\rangle$ . Similarly,  $|H^TR^{-1}(z-h(V))\rangle$  is a normalized quantum state of  $H^TR^{-1}(z-h(V))$ .

The main idea of GQSE is to prepare a quantum superposition of  $\Delta V$ , i.e.,  $|\Delta V\rangle$ , on the quantum circuit, which satisfies (4). To achieve this, since  $H^TR^{-1}H$  is Hermitian, it has a spectral decomposition as follows:

$$\boldsymbol{H}^T \boldsymbol{R}^{-1} \boldsymbol{H} = \sum_{i} \lambda_{j} |u_{j}\rangle \langle u_{j}|, \tag{5}$$

where  $|u_j\rangle$  is the jth eigenvector of  $\boldsymbol{H}^T\boldsymbol{R}^{-1}\boldsymbol{H}$  with respective eigenvalue  $\lambda_j$ .  $|\boldsymbol{H}^T\boldsymbol{R}^{-1}(\boldsymbol{z}-\boldsymbol{h}(\boldsymbol{V}))\rangle$  can also be decomposed using the eigenvectors of  $\boldsymbol{H}^T\boldsymbol{R}^{-1}\boldsymbol{H}$  as follows:

$$|\boldsymbol{H}^T \boldsymbol{R}^{-1} (\boldsymbol{z} - \boldsymbol{h}(\boldsymbol{V}))\rangle = \sum_{j} b_j |u_j\rangle, \tag{6}$$

where  $b_j$  is the coefficient of eigenvector  $|u_j\rangle$ .

Consequently, the quantum superposition of  $\Delta V$ , i.e.,  $|\Delta V\rangle$ , can be established from (4)–(6) as follows:

$$|\Delta V\rangle = (H^T R^{-1} H)^{-1} |H^T R^{-1} (z - h(V))\rangle$$

$$= \left(\sum_j \lambda_j^{-1} |u_j\rangle \langle u_j|\right) \left(\sum_j b_j |u_j\rangle\right)$$

$$= \sum_j \lambda_j^{-1} b_j |u_j\rangle.$$
(7)

(7) allows us to express  $|\Delta V\rangle$  using  $|u_j\rangle$ . The main task is to establish a quantum circuit where  $\lambda_j^{-1}$  is combined with  $b_j|u_j\rangle$ . In the following subsection, the quantum-circuit-based GQSE algorithm is developed to achieve this.

## $2.2. \ \ Quantum\mbox{-}circuit\mbox{-}based\ GQSE\ algorithm$

The architecture of the quantum-circuit-based GQSE algorithm is given in Fig. 1. The overall idea of this algorithm is as follows: The raw data z are measured and sent to the control center to obtain  $H^T R^{-1} H$  and  $H^T R^{-1} (z - h(V))$  in a classical computer.

The HHL quantum circuit is then established to obtain  $|\Delta V\rangle$ . This circuit mainly consists of three components, namely, a quantum phase estimation (QPE), a controlled rotation, and an inverse QPE. The input of this circuit consists of a qubits for ancilla quantum encoding (AQE)

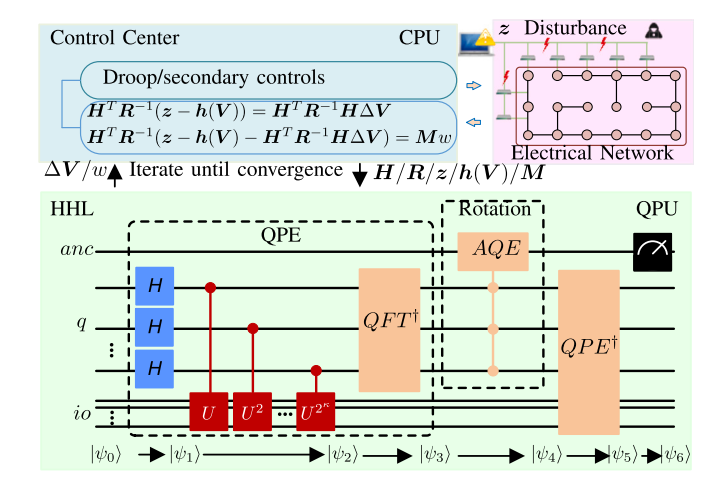


Fig. 1. The architecture of the GQSE algorithm.

(denoted as anc in Fig. 1), n qubits for the binary representation of  $\lambda_j$  (denoted as q in Fig. 1), and m qubits for the binary representation of  $b_j|u_j\rangle$  (denoted as  $i_0$  in Fig. 1). The initialized states  $b_j|u_j\rangle$  ( $j=1,2,\ldots,m$ ) in  $i_0$  can be achieved by applying a set of gates to the initial state  $|0\rangle_m$  [21]. Meanwhile, the eigenvectors in the HHL implementation are prepared in the state  $b_j|u_j\rangle$ . Then, the input of the circuit can be represented as  $|\psi_0\rangle = |0\rangle_n \otimes \sum_j b_j |u_j\rangle_m \otimes |0\rangle_a$ , where  $\otimes$  refers to the tensor product.

The initialized quantum state  $|\psi_0\rangle$  is first handled by QPE. QPE consists of n Hadamard gates for generating quantum superpositions, n quantum unitary gates for obtaining a multi-qubit quantum state containing  $\lambda_j$ , and an inverse quantum Fourier transformation (denoted as  $QFT^{\dagger}$  in Fig. 1) for obtaining each  $\lambda_j$ . The controlled rotation contains a set of controlled quantum gates to obtain the reciprocal of each  $\lambda_j$ , i.e.,  $\lambda_j^{-1}$  [5].  $\lambda_j^{-1}$  and  $b_j|u_j\rangle$  are thus combined through the functions of QPE and the controlled rotation. An inverse QPE (denoted as  $QPE^{\dagger}$  in Fig. 1) is further utilized to reset the state of each qubit in q and  $i_0$ , i.e., making the state of each qubit in q to be zero and that in  $i_0$  as  $b_j|u_j\rangle$ . More details are given below:

QPE

QPE aims to obtain  $\lambda_j$ . To start with, n Hadamard gates are applied on n qubits in q, respectively, to create quantum superpositions. The quantum state (with all the qubits used) after all the Hadamard gates are applied (denoted as  $|\psi_1\rangle$  in Fig. 1), can be expressed as follows:

$$|\psi_1\rangle = H^{\otimes n} \otimes I^{\otimes (m+a)} |\psi_0\rangle$$

$$= \frac{1}{\sqrt{2^n}} \sum_{\alpha \in \{0,1\}^n} |\alpha\rangle_n \sum_j b_j |u_j\rangle_m |0\rangle_a,$$
(8)

where H and I are the Hadamard and unit gates, respectively.

n quantum unitary gates (represented as  $U^{2^\kappa}$  in Fig. 1 where  $\kappa=0,1,\ldots,n-1$ ) are then applied on the qubits in  $i_0$  in series for obtaining a multi-qubit quantum state containing  $\lambda_j$ . Specifically,  $U^{2^\kappa}=e^{(i\pi 2^{\kappa+1}H^TR^{-1}H)}$ . After unitary gates are applied, the quantum state  $(|\psi_2\rangle)$  can be expressed as follows:

$$|\psi_{2}\rangle = \prod_{\kappa=0}^{n-1} U^{2^{\kappa}} \otimes I^{\otimes a} |\psi_{1}\rangle$$

$$= \frac{1}{2^{n/2}} \sum_{\chi=0}^{2^{n}-1} e^{(i2\pi\lambda_{j}\chi)} |\chi\rangle_{n} \sum_{j} b_{j} |u_{j}\rangle_{m} |0\rangle_{a}.$$
(9)

 $QFT^\dagger$  is further applied to obtaining each  $\lambda_j$ . The quantum state after  $QFT^\dagger$  is applied  $(|\psi_3\rangle)$  can be represented as

$$|\psi_3\rangle = QFT^\dagger \otimes I^{\otimes (m+a)} |\psi_2\rangle = \sum_j b_j |\lambda_j\rangle_n |u_j\rangle_m |0\rangle_a. \tag{10}$$

Controlled rotation

AQE is applied to obtaining the reciprocal of each  $\lambda_j$  i.e.,  $\lambda_j^{-1}$ . The quantum state  $(|\psi_4\rangle)$  then contains  $\sum_j \lambda_j^{-1} b_j |u_j\rangle_m$ , i.e.,  $|\Delta V\rangle$  as in (7), as follows:

$$|\psi_4\rangle = AQE \otimes I^{\otimes m}|\psi_3\rangle$$

$$= \sum_j b_j |\lambda_j\rangle_n |u_j\rangle_m (\sqrt{1 - \frac{\beta^2}{\lambda_j^2}} |0\rangle_a + \frac{\beta}{\lambda_j} |1\rangle_a), \tag{11}$$

where  $\beta$  is a user-defined constant value.

Inverse qpe

The inverse QPE  $(QPE^{\dagger})$  is utilized to reset the state of each qubit in q and  $i_0$ . After  $QPE^{\dagger}$  is applied, the quantum state  $(|\psi_5\rangle)$  can be expressed as follows:

$$|\psi_5\rangle = QPE^{\dagger} \otimes I^{\otimes a}|\psi_4\rangle$$

$$= |0\rangle_n \sum_j b_j |u_j\rangle_m (\sqrt{1 - \frac{\beta^2}{\lambda_j^2}} |0\rangle_a + \frac{\beta}{\lambda_j} |1\rangle_a). \tag{12}$$

As shown in (12), once the measurement on anc is  $|1\rangle_a$ , the quantum state can be obtained as:  $|\psi_6\rangle=|0\rangle_n\otimes|\Delta V\rangle_m\otimes|1\rangle_a$ , where  $|\Delta V\rangle_m=\sum_j b_j \frac{\beta}{\lambda_j}|u_j\rangle_m$  (see (7)). The voltage vector V can thus be updated for the next iteration. The aforementioned procedures are required to update at each iteration. The GQSE iterations continue until  $\Delta V$  achieves convergence.

## 3. PQLS for quantum state estimation

Although theoretically HHL offers an exponential speedup in terms of the system dimension, its efficiency can be affected by many factors. The computational complexity of HHL can be expressed as  $O(log(N)\eta^2\kappa^2)$  [12], where  $N, \eta$  and  $\kappa$  respectively denote the dimension, sparsity and condition number of the gain matrix  $H^TR^{-1}H$ . While  $\eta$  does not vary much due to the sparse nature of power grids,  $\kappa$  can largely deviate in different systems. If an ill-conditioned gain matrix  $H^TR^{-1}H$  (where  $\kappa$  is extremely large) appears in GQSE, the efficiency of GQSE will be largely impacted. This is because a larger  $\kappa$  leads to a higher difference between the largest and the smallest eigenvalues, which makes the QPE in GQSE has to have more qubits to maintain the estimation accuracy. This inevitably leads to an increased quantum circuit depth and an over-consumption of qubit resources.

To tackle this challenge, we develop a preconditioned quantum linear solver (PQLS) in this paper. The overall idea of PQLS is to use a preconditioned iterative optimization to obtain  $\Delta V$  instead of directly calculating  $\Delta V$  through (4). In other words, at each iteration in the Gauss–Newton algorithm (see (3) and (4)),  $\Delta V$  is calculated by PQLS which utilizes an optimization process. The iteration procedures of PQLS are given below:

Multiple iterations are involved in PQLS. Here, we use  $\xi$  to distinguish each iteration in PQLS with the iteration in the Gauss–Newton algorithm (denoted as k in (3)), where  $\xi$  starts at 0, and ends until a convergence is reached. At the  $\xi$ th iteration of PQLS,  $\Delta V_{\xi+1}$  and the residual vector  $\mathbf{r}_{\xi+1}$  (i.e.,  $\mathbf{r}_{\xi+1} = \mathbf{H}^T \mathbf{R}^{-1} (\mathbf{z} - \mathbf{h}(\mathbf{V})) - (\mathbf{H}^T \mathbf{R}^{-1} \mathbf{H}) \Delta V_{\xi}$ , obtained from (3)) can be updated by using the gradient descent rule as follows:

$$\begin{cases}
\Delta \boldsymbol{V}_{\xi+1} = \Delta \boldsymbol{V}_{\xi} + \rho_{\xi} \boldsymbol{p}_{\xi} \\
\boldsymbol{r}_{\xi+1} = \boldsymbol{r}_{\xi} + \rho_{\xi} (\boldsymbol{H}^T \boldsymbol{R}^{-1} \boldsymbol{H}) \boldsymbol{p}_{\xi}, \ \xi = 0, 1, \dots
\end{cases}$$
(13)

where the initialized  $\Delta V_{\xi}$  and  $r_{\xi}$  (i.e.,  $\Delta V_0$  and  $r_0$ ) are 0 and  $H^T R^{-1}(z-h(V)) - (H^T R^{-1} H) \Delta V_0$ , respectively.  $p_{\xi}$  refers to the search direction and can be updated as follows:

$$\mathbf{p}_{\xi+1} = \mathbf{w}_{\xi+1} + \mathbf{r}_{\xi+1}^T \mathbf{w}_{\xi+1} (\mathbf{r}_{\xi}^T \mathbf{w}_{\xi})^{-1} \mathbf{p}_{\xi}, \ \xi = 0, 1, \dots$$
 (14)

where  $w_{\xi}$  represents the preconditioned errors [22]. It can be calculated through quantum computing as follows:

$$|\mathbf{r}_{\varepsilon}\rangle = \mathbf{M}|\mathbf{w}_{\varepsilon}\rangle, \ \xi = 0, 1, \dots$$
 (15)

where M denotes a positive-definite, fixed preconditioner. An example of a commonly used preconditioner is the incomplete Cholesky factorization [23].  $\mathbf{w}_{\varepsilon}$  is initialized as follows:

$$|(\boldsymbol{H}^T \boldsymbol{R}^{-1} (\boldsymbol{z} - \boldsymbol{h}(\boldsymbol{V}) - \boldsymbol{H}^T \boldsymbol{R}^{-1} \boldsymbol{H}) \Delta \boldsymbol{V}_0)\rangle = \boldsymbol{M} |\boldsymbol{w}_0\rangle.$$
(16)

 $\mathbf{p}_{\xi}$  is initialized as  $\mathbf{p}_0 = \mathbf{w}_0$ . In (13),  $\rho_{\xi}$  is a coefficient, and can be obtained as  $\rho_{\xi} = \mathbf{r}_{\xi}^T \mathbf{w}_{\xi} (\mathbf{p}_{\xi}^T \mathbf{H}^T \mathbf{R}^{-1} \mathbf{H} \mathbf{p}_{\xi})^{-1} \ (\xi = 0, 1, \ldots)$ .

The entire PQLS algorithm is summarized as follows:

- Step 1: Initialize  $\Delta V_0$ ,  $r_0$ ,  $w_0$ , and  $p_0$ .
- Step 2: For each iteration, update  $\Delta V_{\xi+1}$  and  $r_{\xi+1}$  through (13).
- Step 3: If  $r_{\xi+1}$  reaches a tolerance of  $\epsilon$ , output  $\Delta V_{\xi+1}$ . Otherwise, update  $w_{\xi+1}$  and  $p_{\xi+1}$  using (14) and (15), respectively.

#### 4. EQSE for microgrids

## 4.1. Microgrid hierarchical control

In microgrids, hierarchical controls are applied on DERs to support power consumption and regulate bus voltages [24]. A hierarchical control commonly consists of a droop control and a secondary control. For DC microgrids, a P/V droop control can be applied to balance the power consumption. The main function of the secondary control in this study is to retrieve deviations of local voltages to their nominal values [25,26].

Existing microgrid state estimation methods typically follow classical power flow formulations in (2), which however have ignored the features of hierarchical-control-based microgrids where multiple DERs, instead of a swing bus, support the entire system. Failure to represent the droop/secondary regulation may provide erroneous results when a microgrid is subject to disturbances. In the next subsection, we present the EQSE algorithm considering droop/secondary characteristics.

## 4.2. The EQSE algorithm

The EQSE algorithm is given in Algorithm 1. It incorporates either droop or (droop + secondary) control into h(V) to mitigate errors of state estimation results when the measurement z contains disturbances.

## 4.2.1. Droop-based EQSE

When only droop controls are applied in a microgrid, P(V) and the corresponding elements in the Jacobian matrix H (i.e.,  $\frac{\partial P(V)}{\partial V}$ ) can be devised as

$$\begin{cases} P(V) = GV \circ V + k_G \circ (V_{ref} - V) \\ \frac{\partial P(V)}{\partial V} = GV + G_{(diag)} V - k_G, \end{cases}$$
(17)

where  $G_{(diag)}$  is the diagonal part of G,  $k_G$  is a vector containing the reciprocal of each P/V droop coefficient, and  $V_{ref}$  is the reference-voltage vector.

## 4.2.2. Secondary-based EQSE

When both droop and secondary controls are applied in a microgrid, a dummy bus  $V_d$  can be added to calculate P(V) to assist the voltage recovery. Specifically,  $V_d$  can be designed as  $V_d = V^* - V + V_d^p$ , where V is the unknown-voltage vector,  $V^*$  is the rated-voltage vector, and  $V_d^p$  denotes the dummy-bus-voltage vector at the previous iteration. To be specific, if the element within  $(V^* - V)$  is negative (or positive), the corresponding element in  $V_d^p$  will be added by a positive (or negative) deviation. With the dummy bus  $V_d$ , P(V) and  $\frac{\partial P(V)}{\partial V}$  can be expressed

$$\begin{cases} P(V) = GV \circ V + V \circ (V_d - V) \circ G_d \\ \frac{\partial P(V)}{\partial V} = GV + G_{(diag)}V + (V_d - 2V) \circ G_d, \end{cases}$$
(18)

where  $G_d$  is a vector containing the coefficients. At each iteration,  $V_d$  will be updated until the difference between  $V^*$  and V reaches convergence.

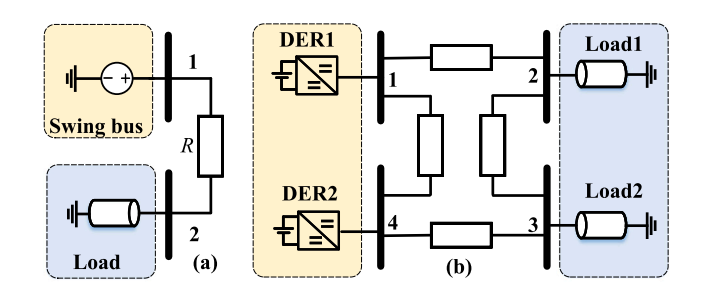


**Fig. 2.** Test system architectures. (a) The 2-bus DC microgrid. (b) The 4-bus DC microgrid.

Note that the aforementioned droop/secondary-based state estimation schemes are discussed in the context of DC microgrids. Nonetheless, the principles of EQSE are generic and can be readily applicable for AC microgrids where hierarchical P/f and Q/V control schemes are adopted.

## Algorithm 1: The EQSE Algorithm

```
Initialize: z, V, V_d, \epsilon, G, G_d, R, M;
while \Delta V, \Delta V_d \geq \epsilon do
     Update: h(V), H, H^T R^{-1} H, H^T R^{-1} (z - h(V)) Eqs. (2), (17) and (18);
     if well-condition then
          Execute: |\psi_0\rangle \xrightarrow{HHL} |\Delta V\rangle, Eq. (4);
     else
          Initialize: \Delta V, r, w, p;
          Update: \Delta V, r, Eq. (13);
          Execute: |\psi_0\rangle \xrightarrow{HHL} |w\rangle Eq. (15) and (16);
           if r < \epsilon then
           | Break;
           end
          Update: p, Eq. (14);
     end
     Update: V, V_d;
Result: V.
```

#### 5. Numerical tests

In the case studies, we validate the correctness of GQSE, PQLS and EQSE in two typical microgrids (see Fig. 2(a) and (b)). The robustness and convergence performance of EQSE are verified as well. All quantum algorithms are implemented in IBM's Qiskit (version: 0.23.4), Terra (version: 0.16.3), and the IBMQ provider (version: 0.11.1). The classical state estimation (i.e., the Gauss–Newton algorithm) is implemented in MATLAB running on a 2.50 GHz computer for comparison.

The base voltage, i.e., the nominal rated voltage of the system, is set at 400 V, and the base power is 1 KVA. In the 2-bus system in Fig. 2(a), Bus 1 is a swing bus whose per-unit bus voltage is fixed at 1 p.u., and supports the power consumption of the entire system. In the 4-bus system in Fig. 2(b), DERs 1 and 2 are connected with Buses 1 and 4, respectively. The P/V droop coefficients for DER 1 and 2 in Fig. 2(b) are set at  $1\times 10^{-5}$  and  $2\times 10^{-4}$ . Each element in  $G_d$  (see (18)) for the secondary control is set at 20.

## 5.1. Validity of gase, PQLS and EQSE

This subsection verifies the correctness of GQSE in the 2-bus system and that of PQLS and EQSE in the 4-bus system. The classical state estimation (CSE), i.e., the Gauss–Newton algorithm [27], is implemented for comparison. Tables 1 and 3 provide the state estimation results of GQSE and PQSL (together with the CSE comparisons) in the normal

**Table 1**GQSE and CSE results in the normal situation (p.u.).

System	Iteration	$V_1$ (GQSE)	$V_2$ (GQSE)	$V_1$ (CSE)	$V_2$ (CSE)
	1	1.0000	0.9486	1.0000	0.9486
2-bus DC grid	2	1.0000	0.9473	1.0000	0.9472
	3	1.0000	0.9472	1.0000	0.9472

**Table 2** GOSE results at 1st iteration with different numbers of qubits in q (p.u.).

Qubits in q	2	4	6	10	CSE
$\Delta V_1$	0.0036	0.0006	0.0004	0.0000	0.0000
$\Delta V_2$	-0.0242	-0.0525	-0.0508	-0.0514	-0.0514

Table 3
PQLS and CSE results in the normal situation (p.u.).

System	Method	Iteration	$\boldsymbol{V}_1$	$\boldsymbol{V}_2$	$V_3$	$V_4$
		1	0.9999	0.9877	0.9884	0.9987
4 h	PQLS	2	0.9999	0.9875	0.9882	0.9986
4-bus DC grid (Droop)		3	0.9999	0.9875	0.9882	0.9986
		1	0.9999	0.9877	0.9884	0.9987
	CSE	2	0.9999	0.9875	0.9882	0.9986
		3	0.9999	0.9875	0.9882	0.9986
4-bus DC grid (Secon- dary)		1	0.9999	0.9880	0.9892	0.9999
	PQLS	2	1.0003	0.9884	0.9895	1.0003
		3	1.0003	0.9884	0.9895	1.0003
		1	0.9999	0.9880	0.9892	0.9999
	CSE	2	1.0003	0.9884	0.9895	1.0003
		3	1.0003	0.9884	0.9895	1.0003

situation (i.e., without an ill-conditioned matrix), respectively. Table 2 gives the state estimation results of GQSE with different numbers of qubits in q (see Fig. 1). Table 4 presents the PQLS and CSE estimation results with an ill-conditioned matrix (i.e., the maximum eigenvalue:  $9.4675 \times 10^{10}$ , and the minimum eigenvalue: 277.7778).

For EQSE, an enhanced state estimation (ESE) method is utilized for comparison. Specifically, ESE has the same principle with EQSE except that the quantum procedures in EQSE are replaced with classical operations. Table 5 presents the comparison results of EQSE and ESE under the droop control and the (droop + secondary) control. From Tables 1–5, the following insights can be obtained:

- The estimation results from GQSE (i.e., after the third iteration) and CSE are exactly the same (see Table 1), which validates the correctness of GQSE.
- For GQSE, having a sufficient number of qubits in q is critical to achieve an accurate estimation result. As shown in Table 2, increasing the number of qubits in q can greatly improve the accuracy of the GQSE result, i.e., the result obtained from GQSE is closer to the CSE result. This is because more precise eigenvalues of  $H^T R^{-1} H$  can be obtained with more qubits in q.
- Tables 3 and 4 validate the correctness of PQLS in the normal situation and with an ill-conditioned matrix, respectively. Results show that even though  $\boldsymbol{H}^T \boldsymbol{R}^{-1} \boldsymbol{H}$  is ill-conditioned, our PQLS-based QSE still possesses excellent convergence by adjusting the preconditioning errors to eventually achieve accurate results.
- Further, Table 5 validates the correctness of EQSE, i.e., the results obtained from EQSE are exactly the same with those from ESE in both droop and secondary controls.

#### 5.2. EQSE against disturbances

This subsection demonstrates the robustness of EQSE against disturbances. Disturbances are assumed to follow the Gauss distribution with

Table 4
GOSE, POLS, and CSE results with an ill-conditioned matrix (p.u.).

Algorithm	Iteration	$\Delta V_1$	$\Delta V_2$	$\Delta V_3$	$\Delta V_4$
GQSE	-	0.0065	-0.0060	-0.0055	0.0049
	1	0.0062	-0.0060	-0.0052	0.0050
	2	0.0062	-0.0060	-0.0052	0.0049
DOI C	3	0.0001	-0.0124	-0.0116	0.0013
PQLS	4	0.0001	-0.0123	-0.0116	0.0013
	5	0.0001	-0.0123	-0.0116	0.0013
	6	0.0001	-0.0123	-0.0116	0.0013
CSE	-	0.0001	-0.0123	-0.0116	0.0013

Table 5
EQSE and ESE results (p.u.).

System	Method	Iteration	$\boldsymbol{V}_1$	$V_2$	$V_3$	$V_4$
	EQSE	1	0.9999	0.9876	0.9884	0.9986
4-bus		2	0.9999	0.9875	0.9883	0.9986
DC grid		3	0.9999	0.9875	0.9883	0.9986
(Droop)	ESE	1	0.9999	0.9876	0.9884	0.9986
-		2	0.9999	0.9875	0.9883	0.9986
		3	0.9999	0.9875	0.9883	0.9986
	EQSE	1	1.0435	1.0317	1.0329	1.0437
		2	1.0018	0.9899	0.9912	1.0020
		3	0.9983	0.9864	0.9877	0.9986
4-bus		4	0.9998	0.9879	0.9892	1.0001
DC grid		5	0.9999	0.9880	0.9893	0.9986 0.9986 0.9986 0.9986 0.9986 1.0437 1.0020 0.9986
(Secon-	ESE	1	1.0435	1.0317	1.0329	1.0437
dary)		2	1.0018	0.9899	0.9912	1.0020
		3	0.9983	0.9864	0.9877	0.9986
		4	0.9998	0.9879	0.9892	1.0001
		5	0.9999	0.9880	0.9893	1.0001

 $N(\mu,\sigma^2)$ . Specifically, 100 samples of disturbances are generated based on the distribution of  $N(0.01,0.01^2)$ . These disturbances are then added to the measurement z, respectively. For each disturbance, EQSE and CSE are used to conduct the state estimation using the updated z (with the disturbance), respectively. Similarly, another 100 samples with the distribution of  $N(0.01,0.05^2)$  are applied. The voltage distributions in droop-based and secondary-based EQSE and CSE under the two distributions are shown in Figs. 3 and 4, respectively, where the outlier, maximum, upper quartile, median, lower quartile, and minimum voltages are presented. Table 6 presents the average voltages and variances (from all the 100 samples) of droop-based and secondary-based EQSE and CSE. It can be observed that:

- The droop-based EQSE outperforms CSE in terms of the robustness against disturbances. For instance, in Fig. 3(a), the voltage distributions of EQSE under the disturbance of  $N(0.01,0.01^2)$  are much narrower than those of CSE. When the disturbance has a distribution of  $N(0.01,0.05^2)$  (see Fig. 3(b)), the voltage variations of CSE become larger, while those of EQSE remain small. This is because CSE relies on a swing bus to balance the disturbances. EQSE then redistributes the disturbances into multiple DERs as it incorporates the hierarchical control scheme. Fig. 4 shows the secondary-based EQSE is also robust against disturbances.
- Table 6 further validates the robustness of both droop-based and secondary-based EQSE under disturbances. For instance, when the disturbance has a distribution of  $N(0.01,0.01^2)$ , for CSE under the secondary control,  $V_1$  becomes 0.9986 p.u., which largely deviates from the value with no disturbance, i.e., 1.0000 p.u. under  $N(0,0^2)$ . However, for EQSE,  $V_1$  remains 0.9998 p.u., i.e., a value much closer to 1.0000 p.u. This becomes more obvious when the disturbance has a distribution of  $N(0.01,0.05^2)$ .

## 5.3. EQSE convergence performance

The EQSE convergence performance is demonstrated in this subsection. Specifically, for both EQSE and CSE, under each disturbance (from

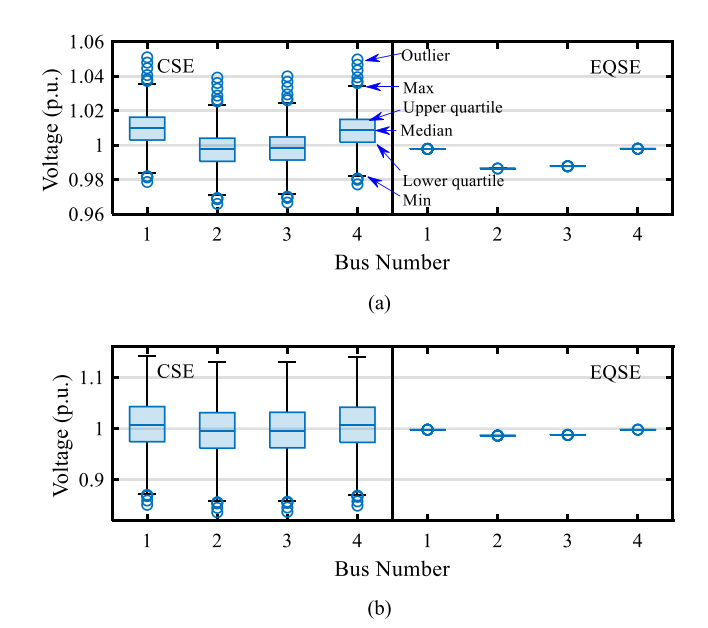


**Fig. 3.** Voltage distribution of droop-based EQSE against disturbances. (a)  $N(0.01, 0.01^2)$ . (b)  $N(0.01, 0.05^2)$ .

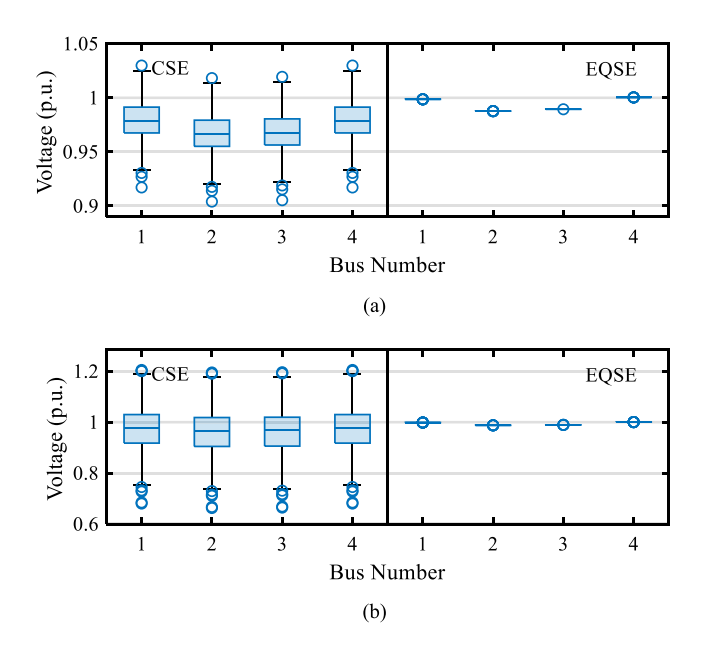


**Fig. 4.** Voltage distribution of secondary-based EQSE against disturbances. (a)  $N(0.01, 0.01^2)$ . (b)  $N(0.01, 0.05^2)$ .

100 samples with  $N(0.01, 0.01^2)$ ), the required number of iterations (for producing the final result) is recorded, in droop-based and secondary-based systems, respectively. The comparison results are given in Fig. 5, from which the following insights can be obtained:

- For either droop-based or secondary-based EQSE, the required number of iterations has a similar level with that of CSE. For instance, all the recorded numbers of iterations for the droop-based EQSE are 4 (see EQSE<sup>1</sup> in Fig. 5), while those for CSE are either 3 or 4 (see CSE<sup>1</sup> in Fig. 5).
- The convergence performance of EQSE is less likely to be affected by disturbances than that of CSE. In Fig. 5, all the recorded numbers of iterations for the droop-based EQSE are 4 (see EQSE<sup>1</sup> in Fig. 5) and those for the secondary-based EQSE are 5 (see EQSE<sup>2</sup> in Fig. 5). However, those for CSE are distributed (see CSE<sup>1</sup> and CSE<sup>2</sup> in Fig. 5).

Table 6
Average EOSE and CSE results with disturbances (p.u.).

Control	Bus Num.	$N(0, 0^2)$	$N(0.01, 0.01^2)$	$N(0.01, 0.05^2)$	
		EQSE&CSE	EQSE/CSE	EQSE/CSE	
	$\boldsymbol{V}_1$	0.9999	0.9980/1.0098	0.9979/1.0110	
Dunn	$\boldsymbol{V}_2$	0.9875	0.9865/0.9976	0.9865/0.9987	
Droop	$V_3$	0.9883	0.9878/0.9983	0.9878/0.9994	
	$V_4$	0.9986	0.9980/1.0085	0.9980/1.0097	
	Variance	-	5.43e-6/1.26e-5	5.55e-6/1.04e-2	
	$V_1$	1.0000	0.9998/0.9986	0.9998/0.9841	
Cocondom	$\boldsymbol{V}_2$	0.9884	0.9877/1.0016	0.9879/0.9719	
Secondary	$V_3$	0.9896	0.9894/1.0028	0.9891/0.9731	
	$V_4$	1.0000	1.0001 /1.0135	0.9999/0.9841	
	Variance		9.75e-4/3.82e-3	1.01e-3/5.20e-3	

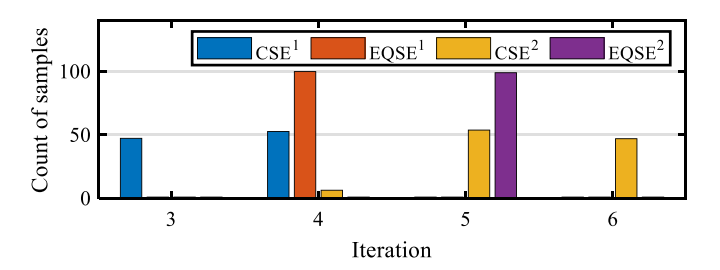


**Fig. 5.** Convergence performances. CSE<sup>1</sup> and EQSE<sup>1</sup>: only with the droop control. CSE<sup>2</sup> and EQSE<sup>2</sup>: with both droop and secondary controls.

#### 6. Conclusion

This paper presents the GQSE formulation for swing-bus-constrained microgrids, and the PQLS for resolving the ill-conditioned matrix issue in GQSE. The EQSE algorithm is further developed for hierarchical-control-based microgrids with exogenous disturbances. Test results demonstrate the correctness of GQSE, PQLS and EQSE in two typical microgrids, and the robustness and convergence performance of EQSE are also verified. Although the two test systems applied in this study have limited scales (due to the fact that current quantum computers still have limitations regarding the quantum depth, coherence time, and noise tolerance capability), the presented methods provide a firm basis, underpinning the great potential of quantum computing in microgrid state estimation.

## CRediT authorship contribution statement

Fei Feng: Algorithm design and software development, Analysis of results, Writing – original draft. Peng Zhang: Principal investigator, Supervision, Conceptualization, Methodology, Formal analysis, Manuscript preparation and editing. Yifan Zhou: Algorithm design, Manuscript proofreading and editing. Zefan Tang: Algorithm design, Writing – review & editing.

## **Declaration of competing interest**

The authors declare that they have no known competing financial interests or personal relationships that could have appeared to influence the work reported in this paper.

#### References

- P. Zhang, B. Wang, P.B. Luh, L. Ren, Y. Qin, Enabling resilient microgrid through ultra-fast programmable network, 2019, US Patent US10505853. [Online].
   Available: https://patents.google.com/patent/US10505853B2/en.
- [2] P. Zhang, Networked Microgrids, Cambridge University Press, Cambridge, UK, 2021.
- [3] A. Primadianto, C. Lu, A review on distribution system state estimation, IEEE Trans. Power Syst. 32 (5) (2017) 3875–3883.

- [4] E. Harmon, U. Ozgur, M.H. Cintuglu, R. de Azevedo, K. Akkaya, O.A. Mohammed, The internet of microgrids: A cloud-based framework for wide area networked microgrids, IEEE Trans. Ind. Inf. 14 (3) (2018) 1262–1274.
- [5] M.A. Nielsen, I.L. Chuang, Quantum Computation and Quantum Information, Cambridge University Press, 2011.
- [6] P. Zhang, W. Krawec, J. Liu, P. Krstic, ASCENT: Quantum Grid: Empowering a Resilient and Secure Power Grid through Quantum Engineering, National Science Foundation, 2020, Proposal# 2023915.
- [7] C. Bravo-Prieto, R. LaRose, M. Cerezo, Y. Subasi, L. Cincio, P.J. Coles, Variational quantum linear solver, 2019, arXiv e-prints, arXiv:1909.05820.
- [8] Y. Subaşı, R.D. Somma, D. Orsucci, Quantum algorithms for systems of linear equations inspired by adiabatic quantum computing, Phys. Rev. Lett. 122 (2019) 060504.
- [9] H.M. Wiseman, G.J. Milburn, Quantum Measurement and Control, Cambridge University Press, 2009.
- [10] A.W. Harrow, A. Hassidim, S. Lloyd, Quantum algorithm for linear systems of equations, Phys. Rev. Lett. 103 (15) (2009) 150502.
- [11] D.W. Berry, A.M. Childs, A. Ostrander, G. Wang, Quantum algorithm for linear differential equations with exponentially improved dependence on precision, Comm. Math. Phys. 356 (3) (2017) 1057–1081.
- [12] D. Dervovic, M. Herbster, P. Mountney, S. Severini, N. Usher, L. Wossnig, Quantum linear systems algorithms: a primer, 2018.
- [13] A. Ambainis, Variable time amplitude amplification and a faster quantum algorithm for solving systems of linear equations, 2010, arXiv e-prints, arXiv: 1010.4458.
- [14] F. Feng, Y. Zhou, P. Zhang, Quantum power flow, IEEE Trans. Power Syst. 36 (4) (2021) 3810–3812.
- [15] Y. Zhou, F. Feng, P. Zhang, Quantum electromagnetic transients program, IEEE Trans. Power Syst. 36 (4) (2021) 3813–3816.

- [16] S. Bi, Y.J. Zhang, Graphical methods for defense against false-data injection attacks on power system state estimation, IEEE Trans. Smart Grid 5 (3) (2014) 1216–1227.
- [17] F. Feng, P. Zhang, Implicit Z<sub>bus</sub> Gauss algorithm revisited, IEEE Trans. Power Syst. 35 (5) (2020) 4108–4111.
- [18] C. Lin, W. Wu, Y. Guo, Decentralized robust state estimation of active distribution grids incorporating microgrids based on PMU measurements, IEEE Trans. Smart Grid 11 (1) (2020) 810–820.
- [19] N. Xia, H.B. Gooi, S. Chen, W. Hu, Decentralized state estimation for hybrid AC/DC microgrids, IEEE Syst. J. 12 (1) (2018) 434–443.
- [20] A. Abur, A. Expósito, Power System State Estimation: Theory and Implementation, in: Power Engineering (Willis), Taylor & Francis, 2004, [Online]. Available: https://books.google.com/books?id=4HM8ngEACAAJ.
- [21] A.C. Vazquez, R. Hiptmair, S. Woerner, Enhancing the quantum linear systems algorithm using Richardson extrapolation, ACM Trans. Quantum Comput. 3 (1) (2022) 1–37, http://dx.doi.org/10.1145/3490631.
- [22] R. Barrett, M. Berry, T. Chan, J. Demmel, J. Donato, J. Dongarra, V. Eijkhout, R. Pozo, C. Romine, H. Van der Vorst, Templates for the solution of linear systems: Building blocks for iterative methods, Math. Comp. 64 (1996).
- [23] P. Concus, G.H. Golub, G. Meurant, Block preconditioning for the conjugate gradient method, SIAM J. Sci. Stat. Comput. 6 (1) (1985) 220–252.
- [24] F. Feng, P. Zhang, Enhanced microgrid power flow incorporating hierarchical control, IEEE Trans. Power Syst. 35 (3) (2020) 2463–2466.
- [25] J.W. Simpson-Porco, Q. Shafiee, F. Dörfler, J.C. Vasquez, et al., Secondary frequency and voltage control of islanded microgrids via distributed averaging, IEEE Trans. Ind. Electron. 62 (11) (2015) 7025–7038.
- [26] F. Feng, P. Zhang, Y. Zhou, Authentic microgrid state estimation, IEEE Trans. Power Syst. 37 (2) (2022) 1657–1660.
- [27] A. Monticelli, State Estimation in Electric Power Systems: A Generalized Approach, Springer Science+Business Media, New York, 2012.